

Far from equilibrium dynamics of tracer particles embedded in a growing multicellular spheroid

Himadri S. Samanta,¹ Sumit Sinha,² and D. Thirumalai¹

¹*Department of Chemistry, University of Texas at Austin, TX 78712*

²*Department of Physics, University of Texas at Austin, TX 78712*

(Dated: December 5, 2021)

By embedding inert tracer particles (TPs) in a growing multicellular spheroid the local stresses on the cancer cells (CCs) can be measured. In order for this technique to be effective the unknown effect of the dynamics of the TPs on the CCs has to be elucidated to ensure that the TPs do not greatly alter the local stresses on the CCs. We show, using theory and simulations, that the self-generated (active) forces arising from proliferation and apoptosis of the CCs drive the dynamics of the TPs far from equilibrium. On time scales less than the division times of the CCs, the TPs exhibit sub-diffusive dynamics (the mean square displacement, $\Delta_{TP}(t) \sim t^{\beta_{TP}}$ with $\beta_{TP} < 1$), similar to glass-forming systems. Surprisingly, in the long-time limit, the motion of the TPs is hyper-diffusive ($\Delta_{TP}(t) \sim t^{\alpha_{TP}}$ with $\alpha_{TP} > 2$) due to persistent directed motion for long times. In comparison, proliferation of the CCs randomizes their motion leading to superdiffusive behavior with α_{CC} exceeding unity. Most importantly, α_{CC} is not significantly affected by the TPs. Our predictions could be tested using *in vitro* imaging methods where the motion of the TPs and the CCs can be tracked.

PACS numbers:

The interplay of systematic short-range forces and non-equilibrium processes arising from cell division and apoptosis give rise to unexpected dynamics in the collective migration of cancer cells [1–7]. An example of relevance here is the invasion of cancer cells (CCs) in a growing multicellular spheroid (MCS), which is relevant in cancer metastasis [6, 7]. Imaging experiments show that the cell dynamics, characterized by a group of cells that remain in contact for a long period, is complex manifesting far from equilibrium characteristics [7–11]. Simulations and theory of minimal models have been used to describe some of the unexpected features observed in the experiments [12–15]. These studies have also established that the dynamics of a growing tumor embedded in an extracellular matrix are spatially highly heterogeneous. The cells in the interior of the solid tumor spheroid undergo sluggish glass-like dynamics whereas those far from the center of the tumor undergo directed faster than diffusive motion [15]. It should be pointed out that explicit introduction of stochastic active forces could also give rise to unusual dynamics in abiotic systems [16–18].

The dynamics of CCs in a growing tumor is determined by the effects of the CC microenvironment on the long time collective migration. The advent of new experimental techniques that probe the local stresses or pressure on the CCs [19–24] have provided insights into the mechanism by which the CCs invade the extracellular matrix. In a recent article, Dolega et. al. [24] developed a method to measure the mechanical stress within MCSs by embedding micron-sized inert deformable polyacrylamide beads (elastic and compressible hydrogel micro-beads) as local stress sensors. The local pressure profiles in the MCS were extracted from the volume changes in the randomly distributed beads by applying osmotic stress. Surprisingly, it was found that the pressure drops at the surface

of the spheroid and increases close to the core of the spheroid.

Inspired in part by this experiment, we used theory and simulations to extract the non-equilibrium collective cell movement during the MCS expansion by following the dynamics of the embedded inert tracer particles (TPs). In our model, a CC grows till it reaches a critical size whereupon it divides into two at a rate k_b . In addition, a randomly chosen CC could undergo apoptosis at a rate, k_a , which is less than k_b . The inequality ($k_a < k_b$), chosen to mimic tumor growth, gives rise to self-generated active forces, making the tumor growth far from equilibrium process [25]. We model the CCs and TPs as deformable objects subject to short-ranged repulsive elastic forces arising from other CCs and TPs, and adhesive attractions involving neighboring CCs and TPs. We investigated the relevant continuum description of the collective behavior of a colony of tracers in the finite as well as in the long time limit, using the Parisi-Wu stochastic quantization method [13, 26–28].

The central results of this study are : (1) The theoretical results show theory that the TPs exhibit sub-diffusive motion in the intermediate time scale ($t \lesssim \frac{1}{k_b}$), with the mean squared displacement, $\Delta_{TP}(t) \sim t^{\beta_{TP}^T}$, with $\beta_{TP}^T = \frac{4}{7}$. In the long time limit, ($t \gtrsim \frac{1}{k_b}$), the TPs undergo hyper-diffusive motion, $\Delta_{TP}(t) \sim t^{\alpha_{TP}^T}$ with $\alpha_{TP}^T = \frac{16}{7}$, in three dimensions. Surprisingly, the value of α_{TP} depends on the form of the short-range interactions between the TPs and CCs, and hence is not universal. (2) In the long time limit, the extent of migration of the TPs relative to CCs is greater, which is reflected in higher α_{TP} compared to CCs, $\alpha_{CC} = 1.45$. The values of both α_{TP} and α_{CC} , obtained using simulations, which uses entirely different forms for the interactions involving both CCs and TPs, are in quantitative agreement with the

theoretical predictions. In contrast, the simulation value for $\beta_{TP}^S (= 0.11)$ is less than the theoretical predictions, likely reflecting substantial differences in the short-range interactions. (3) The dynamics of the CCs and TPs in the intermediate time regime change only quantitatively as the size of the TPs increase. Remarkably, the long time exponents (α_{TP} and α_{CC}) are unaffected as the size of the inert probe particles is increased. This implies that the dynamics of the CCs can be faithfully recovered by following the time-dependent changes in the positions of the TPs, in principle is possible using imaging experiments.

Theory: We assume that the TP and CC dynamics are governed by stochastic equations. The inert (do not divide or undergo apoptosis) but deformable TPs in

a growing tumor spheroid experience systematic short-range volume exclusion interactions arising from other TPs and the CCs. In addition, they are also subject to a random force characterized by Gaussian white noise. The inter CC interactions are modeled by a sum of attractive and repulsive excluded interactions [13]. In order to derive expressions for the mean square displacements, we first obtain an equation for the CC density in terms of $\phi_i(\mathbf{r}, t) = \delta[\mathbf{r} - \mathbf{r}_i(\mathbf{t})]$, and the TP density $\psi_i(\mathbf{r}, t) = \delta[\mathbf{r} - \mathbf{r}_i(\mathbf{t})]$. A closed form Langevin equation for the CC density, $\phi(\mathbf{r}, t) = \sum_i \phi_i(\mathbf{r}, t)$, and the density of TPs ($\psi(\mathbf{r}, t) = \sum_i \psi_i(\mathbf{r}, t)$) may be obtained using the Dean's method [29]. The time evolutions of $\phi(\mathbf{r}, t)$ and $\psi(\mathbf{r}, t)$ are given by,

$$\frac{\partial \psi(\mathbf{r}, t)}{\partial t} = D_\psi \nabla^2 \psi(\mathbf{r}, t) + \nabla \cdot \left(\psi(\mathbf{r}, t) \int_{\mathbf{r}'} [\psi(\mathbf{r}', t) + \phi(\mathbf{r}', t)] \nabla U(\mathbf{r} - \mathbf{r}') \right) + \tilde{\eta}_\psi, \quad (1)$$

$$\frac{\partial \phi(\mathbf{r}, t)}{\partial t} = D_\phi \nabla^2 \phi(\mathbf{r}, t) + \nabla \cdot \left(\phi(\mathbf{r}, t) \int_{\mathbf{r}'} [\psi(\mathbf{r}', t) + \phi(\mathbf{r}', t)] \nabla U(\mathbf{r} - \mathbf{r}') \right) + k_a \phi \left(\frac{k_b}{k_a} - \phi \right) + \sqrt{k_b \phi + k_a \phi^2} f_\phi + \tilde{\eta}_\phi \quad (2)$$

where $\tilde{\eta}_\psi(\mathbf{r}, t) = \nabla \cdot (\eta_\psi(\mathbf{r}, t) \psi^{1/2}(\mathbf{r}, t))$, $\tilde{\eta}_\phi(\mathbf{r}, t) = \nabla \cdot (\eta_\phi(\mathbf{r}, t) \phi^{1/2}(\mathbf{r}, t))$, and $\eta_{\phi, \psi}$ satisfies $\langle \eta_{\phi, \psi}(\mathbf{r}, t) \eta_{\phi, \psi}(\mathbf{r}', t') \rangle = \delta(\mathbf{r} - \mathbf{r}') \delta(t - t')$. The second term in Eq.(1) accounts for the TP-TP interactions ($\nabla \cdot (\psi(\mathbf{r}, t) \int_{\mathbf{r}'} \psi(\mathbf{r}', t) \nabla U(\mathbf{r} - \mathbf{r}'))$) and TP-CC interactions, ($\nabla \cdot (\psi(\mathbf{r}, t) \int_{\mathbf{r}'} \phi(\mathbf{r}', t) \nabla U(\mathbf{r} - \mathbf{r}'))$). The influence of the CCs on the TP dynamics occurs explicitly through the TP-CC coupling. We show below and in more detail in the Supplementary Information (SI) that these two non-linear terms determine the scaling behavior of the dynamical observables for the TPs in both the finite and the long time limit. Similarly, the second term in Eq.(2) contains the CC-CC ($\phi\phi$ fields) and CC-TP interaction ($\phi\psi$) fields.

Because we are interested in the dynamics of the TPs in a growing MCS, we modified the density evolution equation for the CCs phenomenologically by adding a non-linear source term, $\propto \phi(\phi_0 - \phi)$, representing the biological cell birth and apoptosis processes (third term in Eq.(2)), and a non-equilibrium noise term (fourth term in Eq.(2)) that breaks the number conservation of the CCs. The noise, f_ϕ , satisfies $\langle f_\phi(\mathbf{r}, t) f_\phi(\mathbf{r}', t') \rangle = \delta(\mathbf{r} - \mathbf{r}') \delta(t - t')$. The source term, $\propto \phi(\phi_0 - \phi)$, represents the birth and apoptosis events, with $\phi_0 = \frac{k_b}{k_a}$ [30, 31]. The coefficient of f_ϕ , $\sqrt{k_b \phi + k_a \phi^2}$, is the strength of the noise corresponding to number fluctuations, which is a function of the CC concentration. This form has been derived previously [32] using well known methods [33, 34].

Because the equation (Eq. 1), describing the collective motility of the TPs coupled with CCs, violates the fluctuation-dissipation theorem (FDT) due to self-generated forces arising from birth and apoptosis processes, we use the Parisi-Wu [26] stochastic quantization

method to calculate the dynamics of the TPs and CCs. To characterize the dynamics of the TPs, we introduce a fictitious time ' τ_f ', and consider the density and noise fields to be functions of τ_f in addition to the parameters, \mathbf{r} and t . The dynamics in the fictitious time (Eq. (S6) in the SI) requires only the calculation of the response function (G). In this formalism, the correlation function, C is related to G through the FDT relation, which in Fourier space reads, $C = \frac{1}{\omega_{\tau_f}} \text{Im } G$. We can obtain the scaling laws in real space and time from the solution of the density fields in the fictitious time ' τ_f ' variable.

We obtain the following self-consistent equation for the self energy (defined in Eq. (S9) in the SI) from the calculation of the response function:

$$\Delta\nu = \frac{D_\psi k^2}{2\nu} \Sigma(k, \omega, \omega_{\tau_f}), \quad (3)$$

where, $\Delta\nu$ is the correction in ν due to non-linear terms in the equation for the ψ field, and $\nu = D_\psi k^2 + \phi_0 k^2 U(\mathbf{k})$. The self-energy term containing the two-loop contribution from the first order term (containing the two ψ fields in Eq. (S6) in the SI) determine the scaling laws of the observables in the intermediate time. In the long time limit, the long-range density fluctuations associated with the CCs determine the dynamical properties of TPs through CC-TP $\phi\psi$ fields in the fictitious time equation for the ψ variable. We use Eq. (3) to derive the scaling laws for the dynamical observables associated with the TPs.

Simulations: In order to test the theoretical predictions, we simulated a three dimensional MCS with embedded, mobile TPs. As in our previous studies, [12, 14, 15], we used an agent-based model to simulate

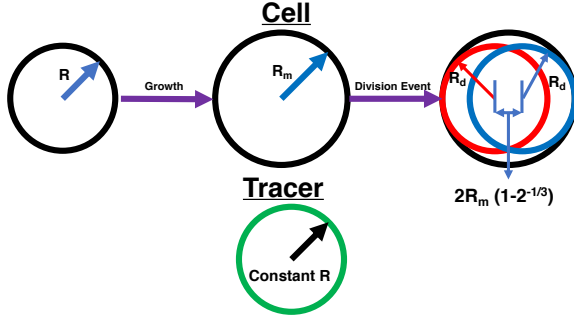


Figure 1: Schematic showing the difference between the CCs (black circle) and TPs (green circle). The CCs undergo growth and division. When the CCs divide they produce two daughter cells with $R_d = \frac{R_m}{2^{1/3}}$, and their relative position is displaced by $R_m(1 - \frac{1}{2^{1/3}})$ with their orientation being random with respect the sphere center. The TPs do not divide and their number is a constant in the simulations.

the dynamics of the TP-CC system. The cells are treated as interacting soft deformable spheres. The CC size increases with time, and divides into two identical daughter cells upon reaching a critical radius (R_m). The mean cell cycle time, measured in units of 15 hrs, is $\frac{1}{k_b}$. The CCs also undergo apoptosis at the rate k_a . However, the sizes and the number of the TPs are constant throughout the simulations.

To study the dynamics of TPs, we account for the CC-CC, CC-TP and TP-TP interactions. We model the interactions using two potentials (Gaussian and Hertz scheme) to ensure that the qualitative results are independent of the nature of the potential (See the details in the SI). The equation of motion governing the dynamics of TP and CCs is taken to be, $\dot{\vec{r}}_i = \frac{\vec{F}_i}{\gamma_i}$, where $\dot{\vec{r}}_i$ is the velocity of i^{th} CC or TP, \vec{F}_i is the force on i^{th} CC/TP, and γ_i represents the damping term (for details see reference [12]). The simulations are performed in the over-damped limit (see [12] and the SI for details).

We used a pressure inhibition mechanism (see the details in SI) to model the observed growth dynamics [12] of the MCS. The CCs can be either dormant or in the growth phase depending on the local microenvironment, which in our model is taken to be the pressure on the i^{th} cell. Figure 1 shows the schematic of growth and division process of the CCs in the absence of the TPs. We argue later that the division event and the subsequent placement of the daughter cells (radius R_d) randomly in space adds a degree of stochasticity in the dynamics of the CCs. We initiated the simulations with 100 TPs and 100 CCs. The spatial coordinates of CCs and TPs were sampled using a normal distribution with mean zero and standard deviation $50 \mu m$.

Results: Both theory and simulations predict that in the limit $t < \frac{1}{k_b}$, the TPs exhibit subdiffusive behavior. The non-linear term $\nabla \cdot (\psi(\mathbf{r}, t) \int d\mathbf{r}' \psi(\mathbf{r}', t) \nabla U(\mathbf{r} - \mathbf{r}'))$ governs the scaling laws. In the spirit of self-consistent

mode coupling theory, we replace ν by $\Delta\nu$ in the self-energy term $\Sigma(\mathbf{k}, \omega, \omega_{\tau_f})$ (Eq.(3)). The momentum count of Eq. (3) with the self-energy term $\Sigma(\mathbf{k}, \omega, \omega_{\tau_f})$ (see Fig. (S6a) in the SI) determines the dynamic exponent $z = 2 + \frac{d}{2}$.

The single cell mean-square displacement (MSD) behaves as, $\Delta(t) = \langle [r(t) - r(0)]^2 \rangle \sim t^{2/z} = t^\beta$. In 3D, $\beta_{TP}^T = \frac{4}{7} = 0.57$ (the superscript T denotes theory), implying that the TPs undergo sub-diffusive motion, which is a characteristic feature of abiotic glass forming systems. The scaling exponent β_{TP}^T depends (explained in the SI) on the form of the interaction potential, which shows that the behavior of MSD in the intermediate time limit is non-universal.

We also simulated the motion of the TPs in a tumor spheroid, and calculated $\Delta_{TP}(t) = \langle [\mathbf{r}(t) - \mathbf{r}(0)]^2 \rangle$ for both the interaction schemes (Gaussian and Hertz potential), using agent-based models. We tracked the positions of all the TPs, and calculated $\Delta_{TP}(t)$ by averaging over ≈ 2000 trajectories. Figure 2 shows $\Delta_{TP}(t)$ using the Gaussian potential and figure S2a in the SI shows $\Delta_{TP}(t)$ using the Hertz scheme. For both the potentials, we observe similar behavior. The plateau in figure 2 increases as the cell cycle time (τ), increases in the intermediate time regime ($t < \tau_{min}$). We find that $\Delta_{TP} \sim t^{\beta_{TP}^S}$ ($\beta_{TP}^S = 0.11$ - the superscript S stands for simulations). Although both theory and simulations produce subdiffusive behavior there is a quantitative difference between β_{TP}^S and β_{TP}^T .

Interestingly, in the limit $t > \frac{1}{k_b}$, theory and simulations predict hyper-diffusive dynamics $\Delta_{TP} \sim t^{\alpha_{TP}}$ with $\alpha_{TP} > 2$. The effect of non-linearity due to the TP-CC interactions coupled with cell birth-apoptosis processes determine the long-time behavior of the TPs. The corresponding self-energy term in Eq.(3), giving rise to the hyper-diffusive dynamics, is shown in Fig.(S6c) in the SI. The momentum count of Eq. (3) with the self-energy term $\Sigma(\mathbf{k}, \omega, \omega_{\tau_f})$ (see Fig.(S6c) in the SI) determines the MSD exponent, which is found to be $\alpha_{TP}^T = 2.28$. The self energy term $\Sigma(\mathbf{k}, \omega, \omega_{\tau_f})$ (Fig(S2c) in the SI) depends linearly on the birth rate for the CCs. The different values for the cell cycle time, i.e., the different values of birth rates do not change the scaling of the self energy term. It only changes the coefficients of the self energy term. Therefore, the MSD exponent for the TPs is independent of the cell cycle time in the long time limit.

The simulation results are in excellent agreement with the theoretical predictions. For times exceeding the cell cycle time, ($t > \tau_{min}$), we observe hyper-diffusive behavior for the dynamics of TPs (see figure 2). For the Gaussian potential, we obtain the MSD exponent $\alpha_{TP}^S \approx 2.3$ (see the inset in figure 2) for the cell cycle time of $0.5\tau_{min}$, τ_{min} and $2\tau_{min}$. Therefore, both theory and simulations show that the TP undergoes hyper-diffusive motion in the long-time limit with α_{TP} being independent of τ_{min} .

The transition from sub-diffusive to hyper-diffusive motion is not sharp (see figure 2). The linear term in the non-linear growth profile ($\propto \phi(\phi_0 - \phi)$) contributes to the

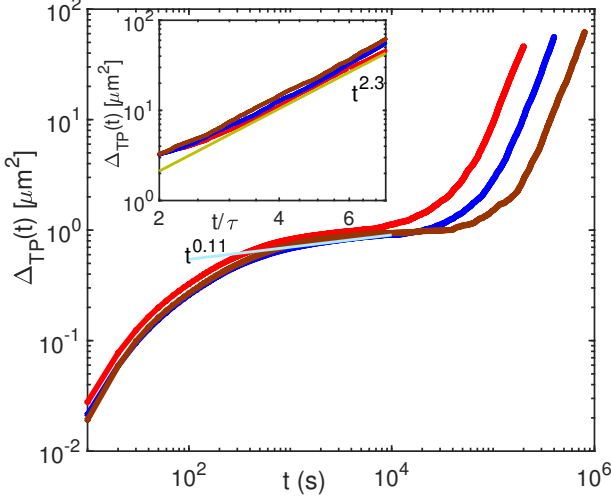


Figure 2: The mean-square displacement of TPs (Δ_{TP}) using the Gaussian potential. The curves are given for 3 different cell cycle time (red ($\tau = 0.5\tau_{min}$), blue ($\tau = \tau_{min}$), and brown ($\tau = 2\tau_{min}$) where $\tau_{min} = 54,000s$). Time to reach the hyper-diffusive behavior, which is preceded by a sub-diffusive regime (i.e. $\Delta_{TP} \sim t^\beta$, $\beta_{cc}^S = 0.11$, shown by the cyan line), increases on increasing τ . In the $t > \tau$ limit, we observe hyper-diffusion. The inset shows Δ_{TP} for the three curves focusing on the hyper-diffusive regime. The x-axis of the inset plot has been scaled by $\frac{1}{\tau}$. The green line in the inset shows the exponent $\alpha_{TP}^S = 2.3$.

TP motion in the transition region, and subsequently the non-linear term in the growth profile determines the dynamics of the TPs in the long-time limit. The momentum count of Eq. (3) with the self-energy term $\Sigma(\mathbf{k}, \omega, \omega_{\tau_f})$ (see Fig. (S2b) in the SI) determines the MSD exponent $\alpha_{TP}^T = 1.33$, implying super-diffusive motion. Therefore, the theoretical result validates the simulations in predicting smooth fluidization transition (Fig. (2)). In the absence of TPs, the birth-apoptosis processes determine the dynamics in CCs. The corresponding MSD exponent $\alpha_{CC} = 1.33$ [13]. In presence of TPs, the CCs exhibit super-diffusive motion with MSD exponent $\alpha_{CC}^T = 1.45$, which is in agreement with the simulation result (figure 3).

Theory and simulations show that α_{TP} exceeds α_{CC} , which we explain by examining the wave vector (k) dependence of the effective diffusion coefficient. For homogeneous systems, without birth or apoptosis, the density obeys Eq. (1) without the non-linear terms. The equilibrium fluctuations ($\langle \delta\psi(\mathbf{k}, t)\delta\psi(\mathbf{k}, 0) \rangle = \psi_0 \exp[-Dk^2t]$) are short-ranged. The diffusion-coefficient (D) is a constant and the MSD exponent is unity. The relaxation time for the time correlation function scales as k^{-z} , with $z = 2$. The deviation from this scaling would be indicative of anomalous diffusion. If we turn on the interactions (short-ranged) between the particles, the intensity of the equal time fluctuations diverges as k^{-z} , the fluctuations become long-

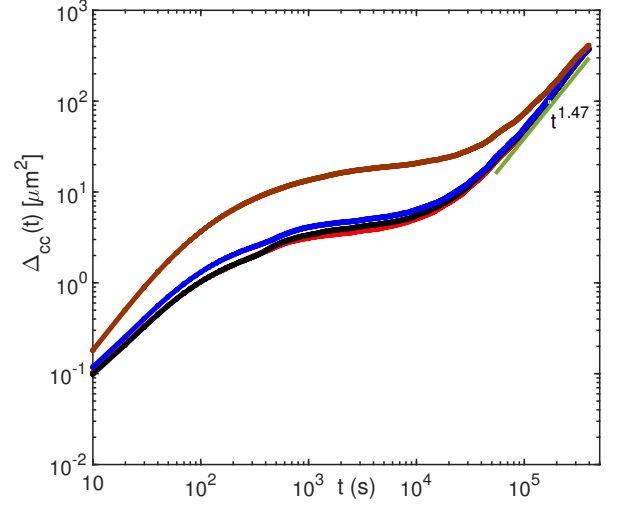


Figure 3: Dynamics of the CCs in the presence of the TPs. The mean-square displacement of the CCs (Δ_{CC}) using the Hertz potential. From top to bottom the curves correspond to different TP radius (brown - $r_{TP} = 2r_c$, blue - $r_{TP} = r_c$, and black - $r_{TP} = 0.75r_c$, and red - $r_{TP} = 0.5r_c$ (appears to be hidden), where $r_c = 4.5\mu m$ corresponds to the average cell radius). The green line serves as a guide to eye for exponent equal to $\alpha_{CC}^S = 1.47$.

range, and non-local extending over the size of the system. In this case, D is k dependent, scaling as k^{z-2} . This is the origin of the anomalous diffusion found here. Depending on the value of z , the CCs and the TPs can exhibit sub or hyper-diffusive motion. The non-linear term in Eq. (1) for the TP-TP interactions renormalizes the diffusion coefficient D . In the intermediate time the correlation function in real space $\langle \delta\psi(\mathbf{r}_1)\delta\psi(\mathbf{r}_2) \rangle$ diverges as $r^{0.5}$ at large separation $r = |\mathbf{r}_1 - \mathbf{r}_2|$. The entire system becomes correlated. The relaxation time for the dynamic structure factor diverges as $k^{-3.5}$, implying that $z = \frac{7}{2}$, resulting in sub-diffusive motion (MSD exponent $\beta_{TP}^T = \frac{z}{2} = \frac{4}{7} \approx 0.57$). The stochastic birth-apoptosis process induces long-range non-equilibrium density fluctuations, which diverge as $k^{-3/2}$, which in turn induces TP density fluctuations ($\sim k^{-7/8}$) through TP-CC interactions. Thus, birth and apoptosis processes produce a dramatic change in the TP density fluctuations (from $k^{-3.5}$ to $k^{-7/8}$). As a result, the MSD exponent $\alpha_{TP}^T \approx \alpha_{TP}^T = 2.28$ in the long-time limit. On the other hand, the presence of TP induces only a minor change in the density fluctuations in the CCs ($\sim k^{-11/8}$). Accordingly, the diffusion coefficients $D_{CC} \sim k^{-5/8}$ for CC and $D_{TP} \sim k^{-9/8}$. The relaxation time associated with the time correlation functions for TPs ($k^{-7/8}$) is small compared to the degree of relaxation time for CCs ($k^{-11/8}$), which implies a higher degree of anomalous diffusion for the TPs.

A mechanistic explanation for $\alpha_{TP} > \alpha_{CC}$ in the long time limit can be gleaned from the simulations. To il-

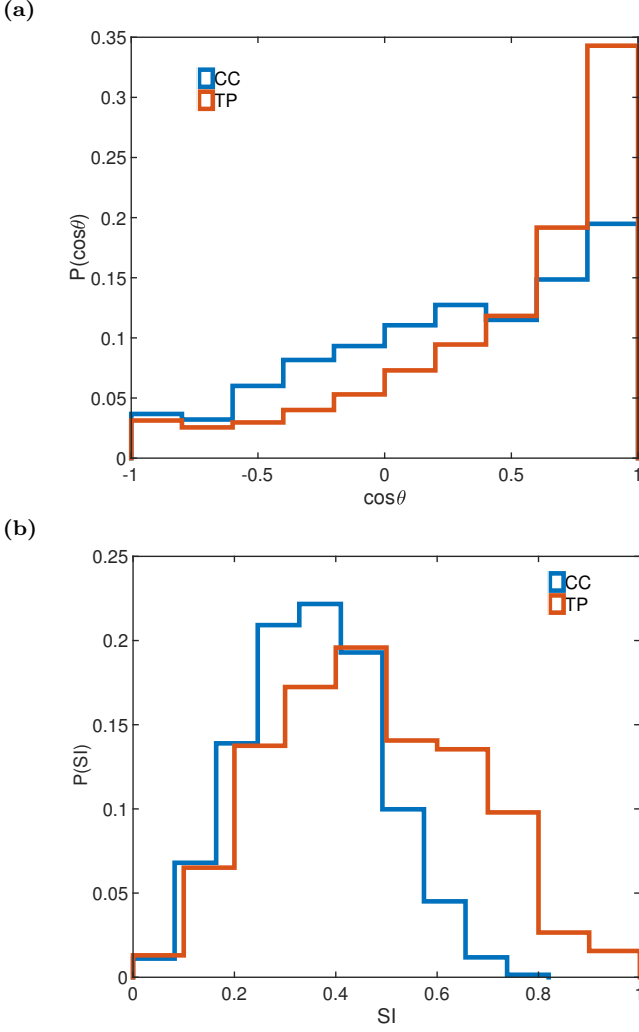


Figure 4: (a) Distribution of $\cos(\theta)$ for the TPs and CCs, where θ is the angle between two consecutive steps along a trajectory. The orange (blue) plot is for TPs (CCs). The distribution is skewed in the positive side (i.e. $\cos(\theta) > 0$) indicative of persistent motion. However, the skewness is more for TPs than CCs and therefore $\alpha_{TP} > \alpha_{CC}$. (b) Distribution of Straightness Index (SI) which measures the rectilinearity of a trajectory. The orange (blue) plot is for TPs (CCs) which shows that the trajectory of TPs is more rectilinear compared to CCs.

illustrate the difference between the dynamics of the TPs and CCs, we calculated the angle (θ) between the trajectory of a CC between two consecutive steps. We define $\cos(\theta(t, \delta t)) = \frac{\delta \mathbf{r}(t+\delta t) \cdot \delta \mathbf{r}(t)}{|\delta \mathbf{r}(t+\delta t)| |\delta \mathbf{r}(t)|}$, where $\delta \mathbf{r}(t) = \mathbf{r}(t + \delta t) - \mathbf{r}(t)$. Figure 4a shows the distribution of an ensemble and time averaged $\cos\theta$ for $\frac{\delta t}{\tau} = 1$. In the absence of any directed motion of the CCs and TPs the distribution of $\cos\theta$ would be uniformly distributed from -1 to 1. However, Figure 4a shows that $P(\cos\theta)$ is skewed towards unity implying that the motion of the TPs and CCs is persistent. As a result of the directed movement, the motion is hyper-diffusive (superdiffusive) for the TPs

(CCs). Because the skewness is more pronounced for the TPs compared to the CCs (Figure 4a) it follows that $\alpha_{TP} > \alpha_{CC}$ in the long time limit.

To further demonstrate that the trajectories of the TPs are more persistent than the CCs, we calculated the Straightness Index (SI), $SI_i = \frac{\mathbf{r}_i(t_f) - \mathbf{r}_i(0)}{\sum \delta \mathbf{r}_i(t)}$. The numerator $\mathbf{r}_i(t_f) - \mathbf{r}_i(0)$ is the net displacement of i^{th} TP or CC, and denominator $\sum \delta \mathbf{r}_i(t)$ is the total distance traversed. Figure 4b clearly demonstrates that TPs trajectories are more straight or persistent over longer duration. The physical reason for the distinct dynamical property of the TPs and CCs is because the CCs undergo proliferation and division. During each cell division, the CCs are placed randomly causing their trajectories to be less persistent. Consequently, $\alpha_{TP} > \alpha_{CC}$, which is predicted by theory and confirmed in the simulations.

Summary: In the present study, using both theory and simulations we probed the out of equilibrium dynamics of TPs embedded in a growing MCS containing cancer cells that undergo cell division and apoptosis. As a consequence of the self-generated active forces due to the CCs the evolving system is driven far away from equilibrium, which in turn produces unexpected and distinct dynamics in the CCs and TPs. We conclude with a few comments. (i) Using a theoretical framework and extensive off-lattice simulations we revealed the complex dynamical properties of both the TPs and CCs in the finite as well as in the long-time limit. The TP-TP interactions determine the sub-diffusive motion in the intermediate times. Interestingly, the long time hyper-diffusive motion of the TPs is a consequence of the biologically relevant events associated with the CCs. Simulations and theory show continuous change from sub-diffusive to hyper-diffusive motions for the TPs. The linear-dependence of the relaxation time on cell-cycle time shows stronger caging effect for higher values of cell-cycle times. The long-time exponent is non-universal, depending on the nature of the interactions. (ii) Although the interactions used in theory and simulations are different the excellent agreement between their predictions, especially in the long time limit, suggests that what determines the collective migration of the CCs is the overall growth law governing tumor expansion. The logistic growth of the tumor arising, in theory, is consistent with what we find in simulations over a range of times, which explains the predicted consistency between theory and simulations. We expect that the dynamics could change dramatically if the tumor growth law is altered, which can be accomplished by changing the ratio of birth and death rates. (iii) Perhaps, most importantly the present work shows that much about the long term dynamics of a collection of CCs could be learned by tracking the movements of embedded inert tracer particles because they do not perturb the CC movements significantly.

Acknowledgements This work is supported by the National Science Foundation (PHY 17-08128 and CHE 16-32756), and the Collie-Welch Chair through the Welch

-
- [1] P. Friedl and D. Gilmour, *Nat. Rev. Mol. Cell Biol.*, 2009, **10**, 445.
- [2] M. Shaebani, A. Wysocki, R. Winkler, G. Gompper and H. Rieger, *Nat. Rev. Phys.*, 2020, **2**, xxx–xxx.
- [3] S. Kumar and V. M. Weaver, *Cancer Metastasis Rev.*, 2009, **28**, 113–127.
- [4] B. Desoize and J.-C. Jardillier, *Crit. Rev. Oncol. Hemat.*, 2000, **36**, 193–207.
- [5] S. Walenta, J. Doetsch, W. Mueller-Klieser and L. A. Kunz-Schughart, *J Histochem Cytochem.*, 2000, **48**, 509–522.
- [6] J. Laurent, C. Frongia, M. Cazales, O. Mondesert, B. Ducommun and V. Lobjois, *BMC cancer*, 2013, **13**, 73.
- [7] A. M. J. Valencia, P.-H. Wu, O. N. Yogurtcu, P. Rao, J. DiGiacomo, I. Godet, L. He, M.-H. Lee, D. Gilkes, S. X. Sun *et al.*, *Oncotarget*, 2015, **6**, 43438.
- [8] R. Richards, D. Mason, R. Levy, R. Bearon and V. See, *bioRxiv*, 2018, 443648.
- [9] N. Martino, S. J. Kwok, A. C. Liapis, S. Forward, H. Jang, H.-M. Kim, S. J. Wu, J. Wu, P. H. Dannenberg, S.-J. Jang *et al.*, *Nat. Photonics*, 2019, **13**, 720–727.
- [10] Y. L. Han, A. F. Pegoraro, H. Li, K. Li, Y. Yuan, G. Xu, Z. Gu, J. Sun, Y. Hao, S. K. Gupta *et al.*, *Nat. Phys.*, 2019, 1–8.
- [11] A. Palamidessi, C. Malinverno, E. Frittoli, S. Corallino, E. Barbieri, S. Sigismund, G. V. Beznoussenko, E. Martini, M. Garre, I. Ferrara *et al.*, *Nat. mater.*, 2019, 1–12.
- [12] A. N. Malmi-Kakkada, X. Li, H. S. Samanta, S. Sinha and D. Thirumalai, *Phys. Rev. X*, 2018, **8**, 021025.
- [13] H. S. Samanta and D. Thirumalai, *Phys. Rev. E*, 2019, **99**, 032401.
- [14] A. Malmi-Kakkada, X. Li, S. Sinha and D. Thirumalai, *arXiv preprint arXiv:1906.11292*, 2019.
- [15] S. Sinha, A. Malmi-Kakkada, X. Li, H. Samanta and D. Thirumalai, *bioRxiv*, 2019, 842930.
- [16] M. C. Marchetti, J.-F. Joanny, S. Ramaswamy, T. B. Liverpool, J. Prost, M. Rao and R. A. Simha, *Rev. Mod. Phys.*, 2013, **85**, 1143.
- [17] C. Bechinger, R. Di Leonardo, H. Löwen, C. Reichhardt, G. Volpe and G. Volpe, *Rev. Mod. Phys.*, 2016, **88**, 045006.
- [18] S. K. Nandi, R. Mandal, P. J. Bhuyan, C. Dasgupta, M. Rao and N. S. Gov, *Proc. Natl. Acad. Sci.*, 2018, **115**, 7688.
- [19] M. Rauzi and P.-F. Lenne, in *Curr. Top. Dev. Biol.*, Elsevier, 2011, vol. 95, pp. 93–144.
- [20] M. S. Hutson, Y. Tokutake, M.-S. Chang, J. W. Bloor, S. Venakides, D. P. Kiehart and G. S. Edwards, *Science*, 2003, **300**, 145–149.
- [21] Y. Boucher, L. T. Baxter and R. K. Jain, *Cancer Res.*, 1990, **50**, 4478–4484.
- [22] H. Fadnes, R. Reed and K. Aukland, *Microvas. Res.*, 1977, **14**, 27–36.
- [23] O. Campàs, T. Mammoto, S. Hasso, R. A. Sperling, D. O’connell, A. G. Bischof, R. Maas, D. A. Weitz, L. Mahadevan and D. E. Ingber, *Nat. Methods*, 2014, **11**, 183.
- [24] M. E. Dolega, M. Delarue, F. Ingremeau, J. Prost, A. Delon and G. Cappello, *Nat. Commun.*, 2017, **8**, 14056.
- [25] A. Doostmohammadi, S. P. Thampi, T. B. Saw, C. T. Lim, B. Ladoux and J. M. Yeomans, *Soft Matter*, 2015, **11**, 7328–7336.
- [26] G. Parisi and Y. S. Wu, *Sci. Sin.*, 1981, **24**, 484.
- [27] H. S. Samanta, J. K. Bhattacharjee and D. Gangopadhyay, *Phys. Letts. A*, 2006, **353**, 113.
- [28] H. S. Samanta and J. K. Bhattacharjee, *Phys. Rev. E*, 2006, **73**, 046125.
- [29] D. S. Dean, *J. Phys. A*, 1996, **29**, L613.
- [30] C. Doering, C. Mueller and P. Smereka, *Physica A*, 2003, **325**, 243.
- [31] A. Gelimson and R. Golestanian, *Phys. Rev. Lett.*, 2015, **114**, 028101.
- [32] H. S. Samanta, M. Hinczewski and D. Thirumalai, *Phys. Rev. E*, 2017, **96**, 012406.
- [33] M. Doi, *J. Phys. A: Math. Ge.*, 1976, **9**, 1465.
- [34] L. Peliti, *J. Phys. (France)*, 1985, **46**, 1469.

Supplementary Information: Far from equilibrium dynamics of tracer particles embedded in a growing multicellular spheroid

Himadri S. Samanta,¹ Sumit Sinha,² and D. Thirumalai¹

¹*Department of Chemistry, University of Texas at Austin, TX 78712*

²*Department of Physics, University of Texas at Austin, TX 78712*

(Dated: December 5, 2021)

Density evolution of TPs and CCs: We begin by considering the dynamics of the tracer particles (TPs) in a growing tumor spheroid. Each TP experiences systematic short-range interactions due to volume excluded from the neighboring TPs and the cancer cells (CCs). In addition, they are also subject to a random force characterized by a Gaussian white noise spectrum. The inter-cell interactions are modeled as a sum of (cadherin-mediated) attractive interactions, and repulsive excluded volume potentials. We assume that the dynamics of the system consisting of the CCs and TPs (see figure S1 for a schematic obtained from simulations) can be described by an overdamped Langevin equation,

$$\frac{\partial \mathbf{r}_i}{\partial t} = - \sum_{j=1}^N \nabla U(|\mathbf{r}_i - \mathbf{r}_j|) + \boldsymbol{\eta}_i(t), \quad (\text{S1})$$

where \mathbf{r}_i is the position of a CC or a TP, and $\boldsymbol{\eta}_i(t)$ is a random force with Gaussian white noise spectrum. To keep the problem theoretically tractable, the form of $U(|\mathbf{r}_i - \mathbf{r}_j|)$ between a pair of particles (can be either TP-TP, TP-CC or CC-CC) was taken to be ,

$$U(|\mathbf{r}(i) - \mathbf{r}(j)|) = \frac{\nu}{(2\pi\lambda^2)^{3/2}} e^{\frac{-|\mathbf{r}(i) - \mathbf{r}(j)|^2}{2\lambda^2}} - \frac{\kappa}{(2\pi\sigma^2)^{3/2}} e^{\frac{-|\mathbf{r}(i) - \mathbf{r}(j)|^2}{2\sigma^2}}, \quad (\text{S2})$$

where, λ and σ are the ranges of the repulsive and attractive interactions, and ν and κ denote the corresponding interaction strengths. Thus, the systematic interactions involving the mixture of CCs and TPs are identical.

When equation S1 is used to characterize the dynamics of the TPs, the potential U_{TP} contains both the TP-TP and TP-CC interactions with the corresponding attractive (repulsive) interaction ranges being $\sigma_1(\lambda_1)$ and $\sigma_2(\lambda_2)$, respectively. The potential U_{CC} for the CCs contains both the cell-cell adhesion and excluded volume interactions, and the CC-TP interactions.

In terms of the density function for a single cell $\phi_i(\mathbf{r}, t) = \delta[\mathbf{r} - \mathbf{r}_i(t)]$, a closed form Langevin equation for the CC density, $\phi(\mathbf{r}, t) = \sum_i \phi_i(\mathbf{r}, t)$ can be obtained using method

introduced by [1]. The time evolution of $\phi(\mathbf{r}, t)$ is given by,

$$\begin{aligned} \frac{\partial \phi(\mathbf{r}, t)}{\partial t} = & \nabla \cdot \left(\phi(\mathbf{r}, t) \int_{\mathbf{r}'} [\psi(\mathbf{r}', t) \nabla U_{CC-TP}(\mathbf{r} - \mathbf{r}') + \phi(\mathbf{r}', t) \nabla U_{CC}(\mathbf{r} - \mathbf{r}')] \right) \quad (\text{S3}) \\ & + D \nabla^2 \phi(\mathbf{r}, t) + \nabla \cdot (\eta_\phi(\mathbf{r}, t) \phi^{1/2}(\mathbf{r}, t)), \end{aligned}$$

where η_ϕ satisfies $\langle \eta_\phi(\mathbf{r}, t) \eta_\phi(\mathbf{r}', t') \rangle = \delta(\mathbf{r} - \mathbf{r}') \delta(t - t')$. Similarly, the evolution of the density function for a single TP, $\psi(\mathbf{r}, t) = \sum_i \psi_i(\mathbf{r}, t) = \sum_i \delta[\mathbf{r} - \mathbf{r}_i(\mathbf{t})]$, may be written as,

$$\begin{aligned} \frac{\partial \psi(\mathbf{r}, t)}{\partial t} = & D_\psi \nabla^2 \psi(\mathbf{r}, t) + \nabla \cdot \left(\psi(\mathbf{r}, t) \int_{\mathbf{r}'} [\psi(\mathbf{r}', t) \nabla U_{TP}(\mathbf{r} - \mathbf{r}') \right. \quad (\text{S4}) \\ & \left. + \phi(\mathbf{r}', t) \nabla U_{TP-CC}(\mathbf{r} - \mathbf{r}')] \right) + \nabla \cdot (\eta_\psi(\mathbf{r}, t) \psi^{1/2}(\mathbf{r}, t)). \end{aligned}$$

where η_ψ satisfies $\langle \eta_\psi(\mathbf{r}, t) \eta_\psi(\mathbf{r}', t') \rangle = \delta(\mathbf{r} - \mathbf{r}') \delta(t - t')$. The second term in Eq.(S4) accounts for the TP-TP/TP-CC interactions. The influence of CCs on the TP dynamics arises explicitly through the second term in Eq.(S4). We show below that these non-linear terms determine the scaling behavior of the dynamical observables for the TPs in both finite and long time limit.

Since, our goal is to study the dynamics of the TPs in a growing spheroid, we extend the density evolution for the CCs phenomenologically by adding a source term describing cell division and apoptosis, and a noise term that breaks the number conservation of the CCs. These terms can be calculated by following the Doi-Peliti formalism [2–4]. The final Langevin equation, for the time-dependent changes in the CC density, $\phi(\mathbf{r}, t)$ is [5],

$$\begin{aligned} \frac{\partial \phi(\mathbf{r}, t)}{\partial t} = & D_\phi \nabla^2 \phi(\mathbf{r}, t) + \nabla \cdot \left(\phi(\mathbf{r}, t) \int d\mathbf{r}' [\psi(\mathbf{r}', t) \nabla U_{CC-TP}(\mathbf{r} - \mathbf{r}') \right. \quad (\text{S5}) \\ & \left. + \phi(\mathbf{r}', t) \nabla U_{CC}(\mathbf{r} - \mathbf{r}')] \right) + k_a \phi \left(\frac{k_b}{k_a} - \phi \right) + \nabla \cdot (\eta_\phi(\mathbf{r}, t) \phi^{1/2}(\mathbf{r}, t)) + \sqrt{k_b \phi + k_a \phi^2} f_\phi, \end{aligned}$$

where f_ϕ satisfies $\langle f_\phi(\mathbf{r}, t) f_\phi(\mathbf{r}', t') \rangle = \delta(\mathbf{r} - \mathbf{r}') \delta(t - t')$. The source term $\propto \phi(\phi_0 - \phi)$, represents the cell birth-apoptosis process, with $\phi_0 = \frac{k_b}{k_a}$ [6, 7]. The coefficient of f_ϕ , given

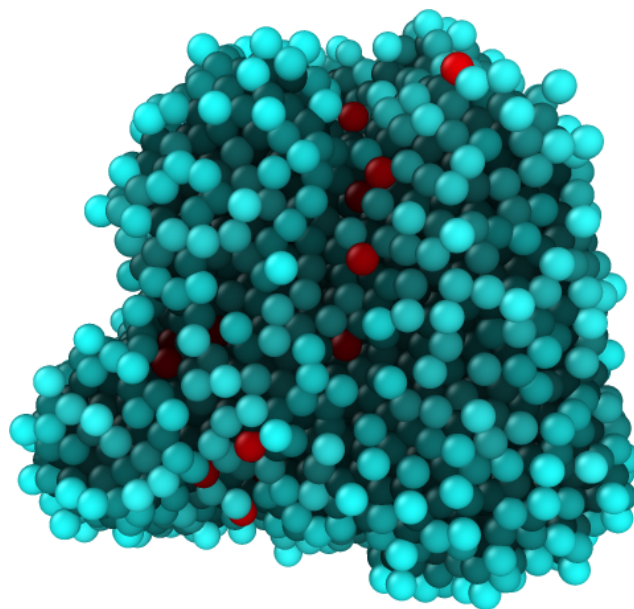
by $\sqrt{k_b\phi + k_a\phi^2}$, is the strength of the noise corresponding to number fluctuations of the CCs, and is a function of the CC density.

A major difficulty in the TP dynamics coupled with CCs arises due to the breakdown of fluctuation-dissipation theorem (FDT) in Eq. (S5). Hence, independent diagrammatic expansions for the response function and the correlation functions are needed. The equilibrium distribution, if it exists at all, is unknown, and the averages can be computed only in the statistical noise. To circumvent these problems, we study the relevant continuum description of collective behavior of a colony of CCs and TPs in the finite as well as in the long-time limit using the stochastic quantization technique [8–10].

To anticipate the consequence of non-linearity in the finite ($t < \frac{1}{k_b}$) and long ($t > \frac{1}{k_b}$) time limit, we introduce a change of scale $\mathbf{r} \rightarrow s\mathbf{r}$, $\psi \rightarrow s^{\chi_1}\psi$, $\phi \rightarrow s^{\chi_2}\phi$ and $t \rightarrow s^z t$, where χ_1 and χ_2 are the exponents corresponding to TP and CC density fluctuations respectively, and z is the dynamic exponent. For $t \lesssim k_b^{-1}$, the scaling of dynamical observables for TPs is governed by the TP-TP and TP-CC interactions. In Fourier space, the non-linear term $(q \cdot (k - q)\psi(q)\psi(k - q))$ for the TP-TP interactions scales (Eq. (S4)) as $q^{2-2\chi_1}$. Similarly, the non-linear term $(q \cdot (k - q)\phi(q)\psi(k - q))$ for the TP-CC interactions scales as $q^{2-\chi_1-\chi_2}$. The degree of non-linearity for both the TP-TP and TP-CC interactions is $q^{2-2\chi_1}$, by noting that $\chi_1 \sim \chi_2$. Therefore, both TP-CC and TP-TP interactions exhibit the same scaling for the dynamical properties of TPs in the $t \lesssim k_b^{-1}$ limit. At long times ($t > \frac{1}{k_b}$), the birth-apoptosis term $\phi(q)\phi(k - q)$ (scales as $q^{-2\chi_2}$), dominates over the short-range CC-CC interactions $q \cdot (k - q)\phi(q)\phi(k - q)$ (scales as $q^{2-2\chi_2}$). Therefore, when $t > \frac{1}{k_b}$, the birth-apoptosis non-linearity determines the scaling properties for the TPs through the TP-CC interactions.

Stochastic quantization approach: To understand the collective dynamics of the

(a)



(b)

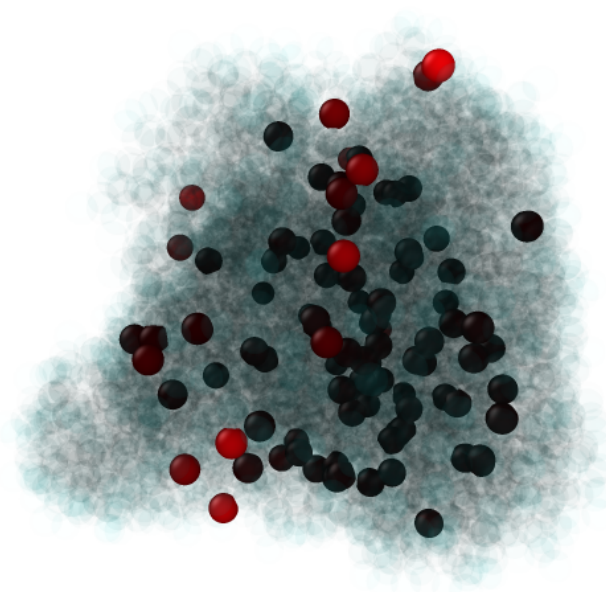


FIG. S1: Snapshot of tumor simulation with embedded tracers. **(a)** A 3D simulated spheroid consisting of approximately 4800 CCs and 100 TPs. The CCs are in cyan, and the tracers are in red. **(b)** The spheroid shown above was rendered by making the CC cells transparent (light colored cyan) in order to show the interior of the spheroid. The TPs are opaque. Some of the TPs appear black because it is a depiction of a 3D image. The purpose of displaying these snapshots is to visually show that the TPs are randomly distributed within the multicellular spheroid, implying that their migration is largely determined by the forces arising from the CCs.

TPs, we use the Parisi-Wu [8] stochastic quantization method developed by in the context of quantum field theory. The collective migration of CCs described by Eq. (S5) is an out of equilibrium process characterized by the absence of FDT, which if valid, would relate the correlation and response function in momentum space by $C = \frac{1}{w} \text{Im}G$. The usual analytic route used to calculate the scaling solution of this problem is to introduce a response field $\tilde{\phi}$. Here, we need to calculate both the response function ($G = \langle \phi \tilde{\phi} \rangle$) and correlation function ($C = \langle \phi \phi \rangle$) separately because of the absence of FDT.

To understand the collective dynamics of the TPs using the stochastic quantization formalism, we introduce the fictitious time ‘ τ_f ’, and consider the density and noise fields to be functions of τ_f in addition to the real parameters, \mathbf{r} and t . The equation of motion for $\Psi(\mathbf{r}, t)$ in the ‘ τ_f ’ variable is,

$$\frac{\partial \Psi(\mathbf{k}, w, \tau_f)}{\partial \tau_f} = -\frac{\delta \mathcal{S}}{\delta \Psi(-\mathbf{k}, -w, \tau_f)} + f_\Psi(\mathbf{k}, w, \tau_f), \quad (\text{S6})$$

with $\langle f_\Psi f_\Psi \rangle = 2\delta(k + k')\delta(w + w')\delta(\tau_f - \tau'_f)$. The field Ψ represents both ψ and ϕ fields. The form of the Langevin equation (S6) ensures that the distribution function will approach $\exp[-S(\mathbf{k}, w)]$ in the $\tau_f \rightarrow \infty$ limit, because FDT is preserved in the τ_f -variable. The action $S(\mathbf{k}, w)$ may be obtained by writing down the joint probability distribution

$P(f_\Psi) \propto \exp[-\int \frac{d^d \mathbf{k}}{(2\pi)^d} \frac{dw}{2\pi} \{ \frac{1}{2(k_a \phi_0 + k_b \phi_0^2 + D_{\phi_1} \phi_0 k^2)} \eta'_\phi(\mathbf{k}, w) \eta'_\phi(-\mathbf{k}, -w) + \frac{1}{(2D_\psi \psi_0 k^2)} \eta'_\psi(\mathbf{k}, w) \eta'_\psi(-\mathbf{k}, -w) \}]$ corresponding to the noise terms η_{ϕ_1} and η_{ψ_1} associated with the CC (Eq.(S5)) and TP equations (Eq.(S4)), respectively. The action $S(\mathbf{k}, w)$ in terms of $\phi(\mathbf{k}, w)$ and $\psi(\mathbf{k}, w)$ may be calculated using Eq.(S5) and Eq.(S4). The expression is too complicated to reproduce here, and is not needed for obtaining the main results. For the simpler case (for a single ϕ field) we have derived it elsewhere [5].

We follow the procedure for obtaining the scaling laws for the systems far from equilibrium, illustrated in the previous studies [5, 9, 10]. The dynamics in Eq.(S6) requires only the calculation of the response function (G) as the correlation function (C) is related to response function through FDT relation, which in Fourier space may be written, as,

$$C = \frac{1}{\omega_{\tau_f}} \text{Im} G. \quad (\text{S7})$$

In order to obtain the scaling laws for the MSD (measurable using particle tracking techniques [11]), it suffices to work at arbitrary but not necessarily $\tau_f \rightarrow \infty$ limit. In the absence of the non-linear terms in Eq. (S6), the Greens function $G_\psi^{(0)}$ (which is the response function) is given by,

$$[G_\psi^0]^{-1} = -i\omega_{\tau_f} + \frac{1}{D_{\psi_1} \psi_0 k^2} [\omega^2 + (D_{\psi_1} k^2 + \psi_0 k^2 U(\mathbf{k}) + \phi_0 k^2 U(\mathbf{k}))^2] \quad (\text{S8})$$

where ω_{τ_f} is the frequency corresponding to the fictitious time τ_f . The effect of non-linear terms can be included perturbatively leading to the Dyson's equation,

$$[G_\psi]^{-1} = [G_\psi^{(0)}]^{-1} + \Sigma_\psi(\mathbf{k}, \omega, \omega_{\tau_f}), \quad (\text{S9})$$

where the self-energy $\Sigma(\mathbf{k}, \omega, \omega_{\tau_f})$ contains the non-linear contributions to the bare Greens function. We obtain the following self-consistent equation for the self energy from the

calculation of response function using Eq.(S6):

$$\Delta\nu = \frac{Dk^2}{2\nu}\Sigma(k, \omega, \omega_{\tau_f}), \quad (\text{S10})$$

where, $\nu = D_\psi k^2 + \phi_0 k^2 U(\mathbf{k})$. The self-energy term, which contains the two-loop contribution from the first order term (containing two ψ fields) in Eq.(S6), contributes to the scaling laws in the intermediate time. In the long time, the second-order term for the ψ equation coupled with non-linearity due to annihilation and cell division produces the scaling exponent. We used Eq.(S10) to derive the scaling laws for the TP dynamics.

Models for Simulations: In order to test the theoretical predictions, we also simulated a three dimensional tumor spheroid with embedded TPs. An agent based model [12–14] is used for the tumor spheroid. The cells are treated as interacting soft deformable objects. The size of the CCs increase dynamically with time, and divides into two identical cells upon reaching a critical mitotic radius (R_m). The mean cell cycle time is τ . In the results section, the cell cycle time τ is expressed in units of $\tau_{min} = 15 \text{ hrs}$. The CCs can also undergo apoptosis. The TPs are assumed to be inert, as in the theory. Therefore, the size and the number TPs are constant throughout the simulations. To study the dynamics of TPs, we include CC-CC, CC-TP and TP-TP interactions. We use two models for the interactions in order to assess the effect of the form of the potential on the dynamics of the TPs and CCs.

Hertz potential: The form of the Hertz forces between the CCs is the same as in our previous work [12, 13], which was adopted from a model introduced in pioneering early studies. [15–17]. The physical properties of the CC, such as the radius, elastic modulus, membrane receptor and ligand concentration characterize the strength of the inter-cellular interactions. The repulsion force, F_{ij}^{el} , accounting for the elastic force between two spheres

with radii R_i and R_j , is given by,

$$F_{ij}^{el} = \frac{h_{ij}^{\frac{3}{2}}}{\frac{3}{4}(\frac{1-\nu_i^2}{E_i} + \frac{1-\nu_j^2}{E_j})(\sqrt{\frac{1}{R_i} + \frac{1}{R_j}})}, \quad (\text{S11})$$

where E_i and ν_i are, respectively, the elastic modulus and poisson ratio of the i^{th} cell. Since, the CCs or the TPs are deformable, the elastic force depends on the overlap, h_{ij} , between two cells. The adhesive force, F_{ij}^{ad} , between the CCs, i and j , is proportional to the area of contact (A_{ij}) [18], which is calculated using [16],

$$F_{ij}^{ad} = A_{ij} f^{ad} \frac{1}{2} (c_i^{rec} c_j^{lig} + c_j^{rec} c_i^{lig}), \quad (\text{S12})$$

where $c_i^{rec}(c_i^{lig})$ is the receptor (ligand) concentration on the surface of the cells, and are taken to be unity in the present study. The coupling constant f^{ad} allows us to scale the adhesive force to account for variable receptor and ligand concentrations.

Repulsive and adhesive forces in Eqs.(S11) and (S12) act along the unit vector \vec{n}_{ij} pointing from the centers of cells j and i . Therefore, the net force on cell i (\vec{F}_i^H) is given by the sum over its nearest neighbors [NN(i)],

$$\vec{F}_i^H = \sum_{j \in NN(i)} (F_{ij}^{el} - F_{ij}^{ad}) \vec{n}_{ij}. \quad (\text{S13})$$

To model the TP-TP and TP-CC interactions, we assume that the TPs are CC-like objects, which mimics experiments [19]. Therefore, CC-TP and TP-TP interactions are the same as CC-CC interactions. As in the theory both F_{ij}^{el} and F_{ij}^{ad} are short range forces because they depend only on h_{ij} , the overlap between CCs.

Gaussian potential: In the theory, we assumed that the CC-CC interaction is given by a sum of Gaussian terms (Eq. (S2)). For this potential, the force \mathbf{F}_{ij}^G on cell i , exerted by cell j , is,

$$\mathbf{F}_{ij}^G = \frac{1}{(2\pi)^{3/2}} \left[\frac{\nu e^{-\frac{r^2}{2\lambda^2}}}{\lambda^5} - \frac{\kappa e^{-\frac{r^2}{2\sigma^2}}}{\sigma^5} \right] \mathbf{r} \quad (\text{S14})$$

where \mathbf{r} is $\mathbf{r}(i) - \mathbf{r}(j)$. We write λ and σ as $\lambda = \tilde{\lambda}(R_i + R_j)$ and $\sigma = \tilde{\sigma}(R_i + R_j)$, as the ranges of interactions corresponding to the repulsive and attractive interaction, respectively. In our simulations, the CCs grow and divide, their radii change in time, and therefore λ and σ also change in time. However, since these interactions are short-ranged, we assume them to be constant (as done in the theory). So, we fixed $\lambda = \tilde{\lambda}(2R_d)$ and $\sigma = \tilde{\sigma}(2R_d)$, where R_d ($\approx 4\mu m$) is the size of a daughter cell (introduced in the next section). For simplicity, we write force $\mathbf{F}_{ij}^G = [\frac{\tilde{\nu}e^{-\frac{r^2}{2\lambda^2}}}{\lambda^2} - \frac{\tilde{\kappa}e^{-\frac{r^2}{2\sigma^2}}}{\sigma^2}]\mathbf{r}$, where $\tilde{\nu} = \frac{1}{(2\pi)^{3/2}}\frac{\nu}{\lambda^3}$ and $\tilde{\kappa} = \frac{1}{(2\pi)^{3/2}}\frac{\kappa}{\sigma^3}$. In the simulations, we fixed $\tilde{\nu} = 0.03$, $\tilde{\lambda} = 0.28$, $\tilde{\kappa} = 0.003$ and $\tilde{\sigma} = 0.4$.

Equation of Motion: The equation of motion governing the dynamics of TP and CCs is taken to be,

$$\dot{\vec{r}}_i = \frac{\vec{F}_i}{\gamma_i}, \quad (\text{S15})$$

where $\dot{\vec{r}}_i$ is the velocity of i^{th} CC or TP, \vec{F}_i is the force on i^{th} CC/TP (see equation S13 and S14), and γ_i represents the damping term (for details see reference [12]).

Cell division: The division process of CCs is taken into account using a pressure inhibition mechanism. The CCs are either dormant or in the growth phase depending on the value of the pressure. The pressure on cell i (p_i) due to $NN(i)$ neighboring cells is calculated using the Irving-Kirkwood equation,

$$p_i = \frac{1}{3V_i} \sum_{j \in NN(i)} \mathbf{F}_{ij} \cdot d\mathbf{r}_{ij}, \quad (\text{S16})$$

where \mathbf{F}_{ij} is the force on i^{th} cell due to j^{th} cell and $d\mathbf{r}_{ij} = \mathbf{r}_i - \mathbf{r}_j$. The volume of the i^{th} cell (V_i) is $\frac{4}{3}\pi R_i^3$, where R_i is the radius of the i^{th} cell. If p_i exceeds a pre-assigned critical limit p_c ($= 1.7 \times 10^{-6}$ MPa) the CC enters a dormant phase. The dormancy criterion serves as a source of mechanical feedback, which limits the growth of the tumor spheroid [20–24]. The volume of a growing cell increases at a constant rate, r_V . The cell radius is updated from a

Gaussian distribution with the mean rate $\dot{R} = (4\pi R^2)^{-1} r_V$. Over the cell cycle time τ ,

$$r_V = \frac{2\pi(R_m)^3}{3\tau}, \quad (\text{S17})$$

where R_m is the mitotic radius. A cell divides once it grows to the fixed mitotic radius. To ensure volume conservation, upon cell division, we use $R_d = R_m 2^{-1/3}$ as the radius of the daughter cells. The resulting daughter cells are placed at a center-to-center distance $d = 2R_m(1 - 2^{-1/3})$ (Fig. 1 in the main text). The direction of the new cell location is chosen randomly from a uniform distribution on a unit sphere.

We initiated the simulations with 100 TPs and 100 CCs. The coordinates of the CCs and TPs were sampled using a normal distribution with mean zero and standard deviation $50 \mu m$. The initial radii of the CCs and TPs were sampled from a normal distribution with mean $4.5 \mu m$, and standard deviation $0.5 \mu m$. Hence, the CCs and TPs are polydisperse cells.

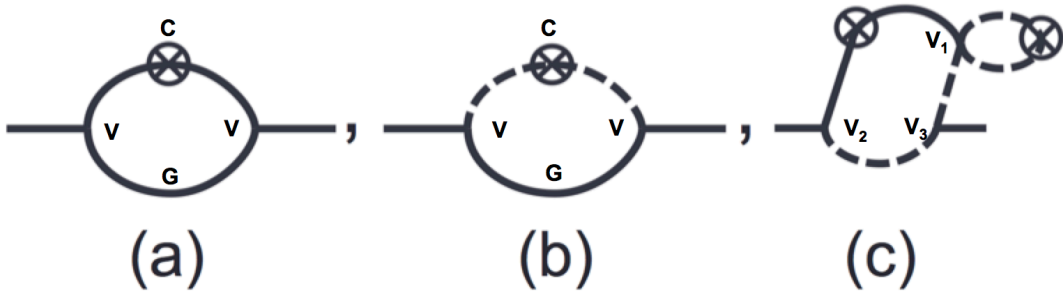


FIG. S2: Diagrammatic representations of the self-energy terms contributing to sub-diffusive (a), super-diffusive (b) and hyper-diffusive (c) behaviors. The solid line represents the full Greens function for the tracer and the dotted line represents the full Greens function for the cell. The line with a crossed circle represents the full correlation function.

TPs exhibit subdiffusive dynamics in the intermediate time regime ($t \lesssim k_b^{-1}$):

At $t < \frac{1}{k_b}$, the non-linear term $\nabla \cdot (\psi(\mathbf{r}, t) \int d\mathbf{r}' \psi(\mathbf{r}', t) \nabla U(\mathbf{r} - \mathbf{r}'))$, describing the TP-TP interactions, governs the scaling laws. In the spirit of self-consistent mode coupling theory, we replace ν by $\Delta\nu$ in the self-energy term $\Sigma(k, \omega, \omega_{\tau_f})$ (Eq.(S10)). According to the scale transformation, we find $\omega \sim k^z$, $\omega_{\tau} \sim k^{2z-2}$, $G_{\psi} \sim k^{-2z+2}$, $C_{\psi} \sim k^{-4z+4}$, and the vertex factor $V \sim k^z$. The form of V is $\frac{1}{(D_{\psi_1} \psi_0 k^2)} (\{i\omega + Dk^2 + \phi_0 k^2 U(\mathbf{k})\} \{(-\mathbf{k}' \cdot \mathbf{k}) U(\mathbf{k}')\} + \{i\omega' + D_{\phi_1} k'^2 + \phi_0 k'^2 U(\mathbf{k}')\} \{(-\mathbf{k}' \cdot \mathbf{k}) U(-\mathbf{k})\} + \{i\omega' + D_{\phi_1} k'^2 + \phi_0 k'^2 U(\mathbf{k}')\} \{(-\mathbf{k}' \cdot (\mathbf{k} - \mathbf{k}')) U(\mathbf{k} - \mathbf{k}')\})$. Self energy term (shown in fig.(S2a)) has the form: $\Sigma(\mathbf{k}, \omega, \omega_{\tau_f}) \sim \int \frac{d^d \mathbf{k}'}{(2\pi)^d} \frac{d\omega'}{2\pi} \frac{d\omega_{\tau'}}{2\pi} V V G C$. By carrying out the momentum count of $\Sigma(\mathbf{k}, \omega, \omega_{\tau_f})$, and keeping in mind that $\Delta\nu \sim k^z$, we find $\Sigma(\mathbf{k}, \omega, \omega_{\tau_f}) \sim k^{d-z+4}$. Using Eq. (S10), we obtain $k^z \sim k^{d-z+4}$, which leads to $z = 2 + \frac{d}{2}$.

The single cell mean-square displacement behaves as,

$$\langle [r(t) - r(0)]^2 \rangle \sim t^{2/z} = t^{\alpha_{TP}} \quad (\text{S18})$$

Therefore, in the intermediate time regime, $\beta_{TP}^T = \frac{2}{z} = 0.57$, implying that the TPs undergo sub-diffusive motion, which is a characteristic feature of glassy systems. The $\beta_{TP}^T = 0.57$ value holds provided the interaction potentials involving the CCs and TPs are given by Eq. S2. On the other hand, if the TP-TP interaction is modeled as $U_1 = U_0 / \cosh^2(r/a)$ instead of a Gaussian (Eq.(S2)), we obtain $\beta_{TP}^T = \frac{4}{8} = 0.5$.

The reason for the dependence on the interactions is that the non-linear term $\int d\mathbf{q} (-\mathbf{q} \cdot \mathbf{k}) U(\mathbf{q}) \psi_1(\mathbf{q}) \psi_1(\mathbf{k} - \mathbf{q})$ involving the TP-TP interactions, determines the scaling exponent in the intermediate time scale. For the Gaussian potential, $U(\mathbf{q}) = \exp[-q^2/2\sigma^2]$, which has no explicit q dependence. For the potential of the form $U_1 = U_0 / \cosh^2(r/a)$, $U(\mathbf{q}) = a^2 q \sqrt{\pi/2} \cosh(aq\pi/2)$, i.e., $U(\mathbf{q})$ has explicit q dependence, which is reflected in the different scaling exponents for different potential form. In this case $\beta_{TP}^T = 4/8 = 0.5$. Regardless of the nature of the potentials, as long as they are short-ranged, the intermediate value of β_{TP} is less than unity, indicating glass-like dynamics in the intermediate time scales ($t < k_b^{-1}$).

Hyper-diffusion in the long time limit: In the log-time limit ($t \gg k_b^{-1}$), the effects of non-linearity due to TP-CC interactions coupled with cell birth-apoptosis process, determine the scaling laws for the TP dynamics. The corresponding self-energy term in Eq.(S10) is shown in Fig.(S2c). We use the scale transformations: $\omega \sim k^z$, $\omega_{\tau} \sim k^{2z-2}$, $G_{\psi} \sim k^{-2z+2}$, $C_{\psi} \sim k^{-4z+4}$, $G_{\phi} \sim k^{-2z}$, $C_{\phi} \sim k^{-4z}$, and vertex factors $V_1 \sim k^2$ and $V_{2,3} \sim k^z$ for Gaussian interaction. Now $\Delta\mu \sim k^z$, we find $\Sigma(\mathbf{k}, \omega, \omega_{\tau_f}) \sim \int \frac{d^d \mathbf{k}'}{(2\pi)^d} \frac{d\omega'}{2\pi} \frac{d\omega'_{\tau_f}}{2\pi} V_1 V_2 V_3 G_{\psi} G_{\psi} C_{\phi} C_{\psi} \sim k^{d+4-7z}$. From the self-consistent equation (Eq. (S10)) we find that the dynamic exponent, $z = (d+4)/8$. The MSD exponent $\alpha_{TP}^T = \frac{2}{z} = \frac{16}{7} = 2.28$, implying hyper-diffusive motion. The self energy term $\Sigma(\mathbf{k}, \omega, \omega_{\tau_f})$ (Fig(S2c)) depends linearly on the birth rate for the CCs. The different values for the cell cycle time, i.e., the different values of birth rate (k_b), do not change the scaling of the self energy term. It only changes the coefficients of the self energy term. Therefore, the MSD exponent for the TPs is independent of the cell cycle time as long as t is large.

The transition from sub-diffusive to hyper-diffusive motion is not sharp (see the Fig.(S3a) and (S3b)). Before cell division time ($t \ll k_b^{-1}$), the TP-TP interactions ($\nabla \cdot (\psi(\mathbf{r}, t) \int d\mathbf{r}' \psi(\mathbf{r}', t) \nabla U(\mathbf{r} - \mathbf{r}'))$) determine the dynamics of TPs. At $t \simeq k_b^{-1}$, the density of CCs started growing and the TP-CC interactions ($\nabla \cdot (\psi(\mathbf{r}, t) \int d\mathbf{r}' \phi(\mathbf{r}', t) \nabla U(\mathbf{r} - \mathbf{r}'))$) determine the TP-dynamics. According to the scale transformation, we use $\omega \sim k^z$, $\omega_{\tau_f} \sim k^{2z-2}$, $G_{\psi} \sim k^{-2z+2}$, $C_{\psi} \sim k^{-4z+4}$, $G_{\phi} \sim k^{-2z}$, $C_{\phi} \sim k^{-4z}$, and vertex factor $V \sim k^z$. Self energy term has the form: $\Sigma(\mathbf{k}, \omega, \omega_{\tau_f}) \sim \int \frac{d^d \mathbf{k}'}{(2\pi)^d} \frac{d\omega'}{2\pi} \frac{d\omega'_{\tau_f}}{2\pi} V V G_{\psi} C_{\phi}$ (See fig.(S2b)). By carrying out the momentum count of $\Sigma(\mathbf{k}, \omega, \omega_{\tau_f})$, we find $\Sigma(\mathbf{k}, \omega, \omega_{\tau_f}) \sim k^{d-z}$. Using Eq.(S10), we find $k^z \sim k^{d-z}$, which leads to $z = \frac{d}{2}$. In this regime, $\alpha_{TP}^T = \frac{4}{3} = 1.33$, implying super-diffusive motion. For the time $t \gg k_b^{-1}$, the non-linear term in the growth profile ($k_b \phi^2$ in Eq. (S5)) contributes to the dynamics of TPs through the TP-CC interactions and TPs

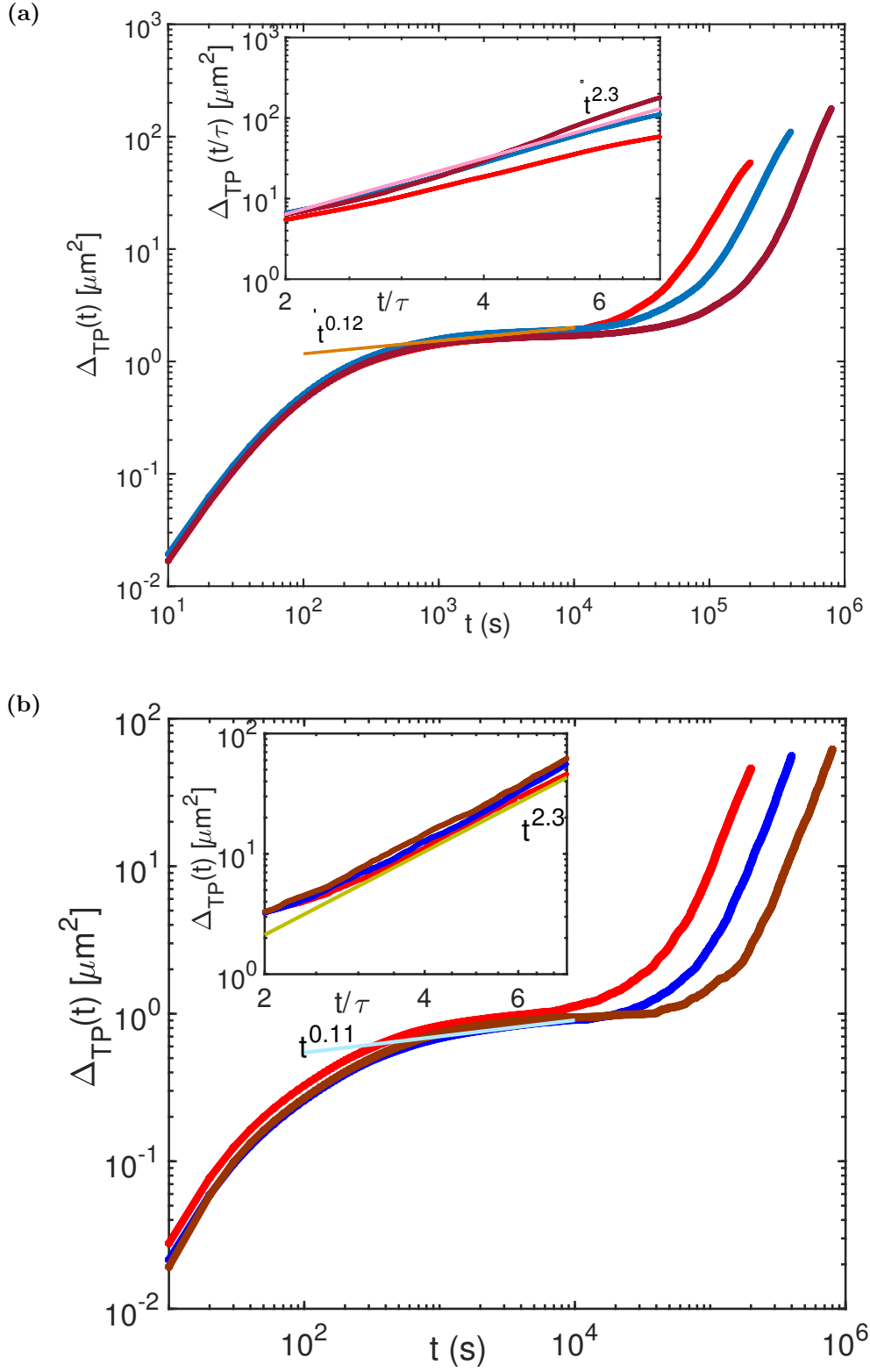


FIG. S3: Mean Square displacement($\Delta_{TP}(t)$) of the TPs as a function of time (t) for the two types of CC interactions. **(a)** Δ_{TP} calculated using Eq. S13 for the forces between the CCs and TPs. The curves correspond to 3 values of τ (continued on the next page)

FIG. S3: (red for $\tau = 0.5\tau_{min}$, blue for $\tau = \tau_{min}$ and brown for $\tau = 2\tau_{min}$, where $\tau_{min} = 54,000s$). Time taken to reach the super-diffusive regime, which is preceded by a sub-diffusive regime, increases as τ increases. In the long-time ($t > \tau$), $\Delta_{TP}(t)$ undergoes hyper-diffusive motion ($\Delta_{TP} \sim t^{\alpha_{TP}^S}$ with $\alpha_{TP}^S > 2$), which is highlighted in the inset. The inset shows Δ_{TP} for the three curves focusing on the super-diffusive regime. The x-axis of the inset plot is scaled by $\frac{1}{\tau}$. The pink line in the inset corresponds to an exponent $\alpha_{TP}^S = 2.3$ (b) Same as (a) except the Gaussian potential (equation S14) is used in the simulations. Interestingly, α_{TP}^S does not change appreciatively.

show hyper-diffusive motion. Therefore, the theoretical result validates the simulations in predicting smooth fluidization transition (Fig.(S3a)).

Scaling of the effective diffusion coefficient: The theory predicts that MSD exponent (α_{TP}) for TP is larger than α_{CC} for CC in the long-time limit. For homogeneously distributed TPs, the density fluctuation obeys the Eq.(S4) without the non-linear terms. The equilibrium fluctuations, ($\langle \delta\psi(k, t)\delta\psi(k, 0) \rangle = \psi_0 \exp[-Dk^2t]$) are short-ranged and decay exponentially. The intensity of the equal-time fluctuations is independent of the wavenumber, k . The diffusion-coefficient (D) is a constant, and the MSD exponent is unity. The relaxation time ($(Dk^2)^{-1}$) for the time correlation function ($\langle \delta\psi(k, t)\delta\psi(k, 0) \rangle$) scales as k^{-z} , with $z = 2$. The deviation from this scaling would indicate the emergence of anomalous diffusion. If we turn on the interactions (short-ranged) between the particles, the diffusion-coefficient ($D(k)$) becomes k dependent, and scales as k^{z-2} . The interactions between the CCs and TPs modify the density fluctuations, giving rise to an effective k -dependent diffusion coefficient. This is the origin of anomalous diffusion for the TPs and CCs. Depending on the value of z , the TPs and CCs could exhibit either sub or super-

diffusive motion. The non-linear term in Eq. (S4) for the TP-TP interactions renormalizes the diffusion coefficient D . The effective diffusion for TPs, $D_{TP} \sim k^{z-2} = k^{-9/8}$, and for CCs the diffusion coefficient $D_{CC} \sim k^{-5/8}$. The ratio $D_{TP}/D_{CC} \sim k^{-1/2}$. In the $k \rightarrow 0$ limit, $D_{TP} > D_{CC}$. The relaxation time scale for the dynamic structure factor for TPs ($k^{-7/8}$) is small compared to the relaxation time for CCs ($k^{-11/8}$), and thus indicating a higher degree of anomalous diffusion for TPs.

Long time MSD exponent is nearly independent of the TP size: To further understand the properties of long time dynamics of the TPs, we varied the radius of the TP (r_{TP}) from $0.5r_c$ to $2r_c$, where $r_c = 4.5\mu m$ is the average CC radius. Figure S4 shows $\Delta_{TP}(t)$ using the Hertz interaction scheme (Eq. (S13)). We observe approximately similar behavior for both the interaction schemes. In the intermediate time regime, TPs with larger radius have higher MSD, because TPs experience large repulsive forces due to enhanced excluded volume interactions. In the long time limit, Δ_{TP} exhibits hyper-diffusion. The exponents vary slightly from 2 to 2.3, which shows that the TP radius does not influence the long time exponent significantly. The CC-TP interaction term, $\nabla \cdot (\psi(\mathbf{r}, t) \int d\mathbf{r}' \phi(\mathbf{r}', t) \nabla U(\mathbf{r} - \mathbf{r}'))$, in Eq.(S4) shows that the radius only alters the interaction strength, and does not fundamentally alter the scaling behavior. The conclusion that the values of α_{TP} do not change, anticipated on theoretical grounds, is also supported by simulations.

Influence of the TP size on the CC dynamics: We calculated the mean square displacement, $\Delta_{CC}(t)$ using the Hertz scheme (equation S13) as a function of the TP radius (figure S5). The values of $\Delta_{CC}(t)$ for $t < \tau_{min}$ is greater as the TP sizes increase. Before the CCs divide, the number of CCs and TPs are similar, which explains the influence of the TPs on the dynamics of CCs in the intermediate time regime. The larger TPs undergo strong repulsion (the repulsive interaction is proportional to R^2) initially, which enhances

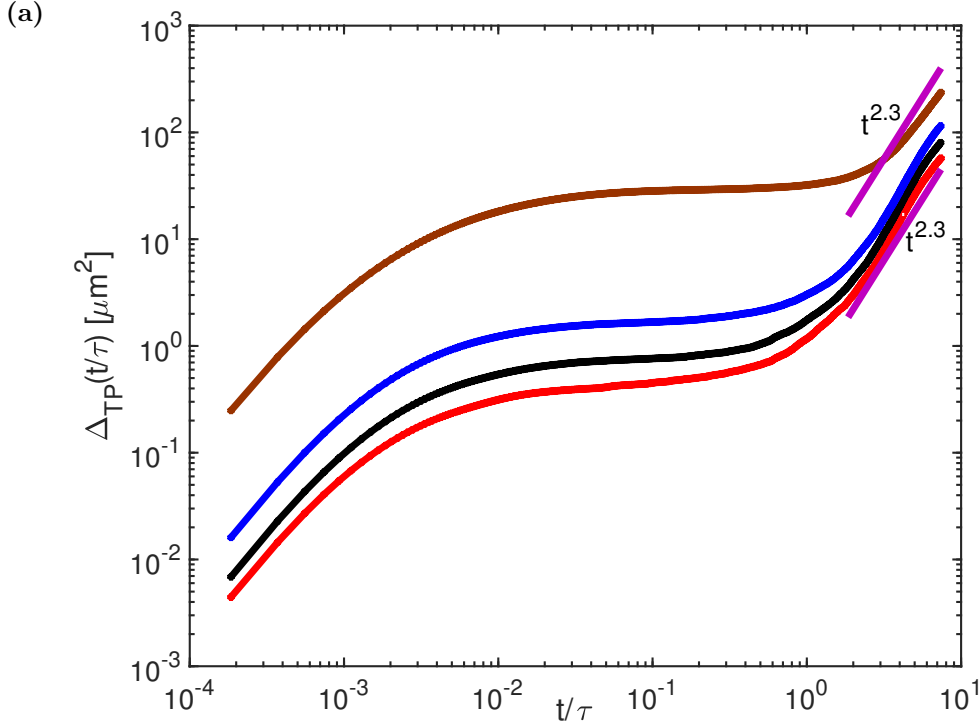


FIG. S4: Dependence of the TP size on the motility. **(a)** The mean-square displacement of TPs (Δ_{TP}) using the Hertz forces between the CCs (see equation S11-S13). The x-axis has been scaled by $\frac{1}{\tau}$ with $\tau = 54,000s$. From top to bottom, the curves correspond to decreasing TP radius ($r_{TP} = 2r_c$ (brown), $r_{TP} = r_c$ (blue), black for $r_{TP} = 0.75r_c$ (black) and $r_{TP} = 0.5r_c$ (red), where $r_c = 4.5\mu m$ corresponds to average cell radius). TPs with larger radius have larger MSD in the intermediate time ($\frac{t}{\tau} \leq \mathcal{O}(1)$). Two magenta lines serve as guide to eye for exponent $\alpha_{TP}^T = 2.3$ as the TP radius increases. The long-time dynamics is hardly affected by the CC-TP interactions (see figure S5). In the absence of the TPs, CCs exhibit super-diffusion where MSD scales as $t^{\alpha_{CC}}$ with $\alpha_{CC} = 1.33$. In the presence of the TPs, CCs also exhibit super-diffusion with increase in the value of α_{CC}^T to 1.45. The simulation result agrees well with the theoretical prediction in the long-time limit.

An important finding, both in the theory and the simulations, is that $\alpha_{TP} > \alpha_{CC}$. For

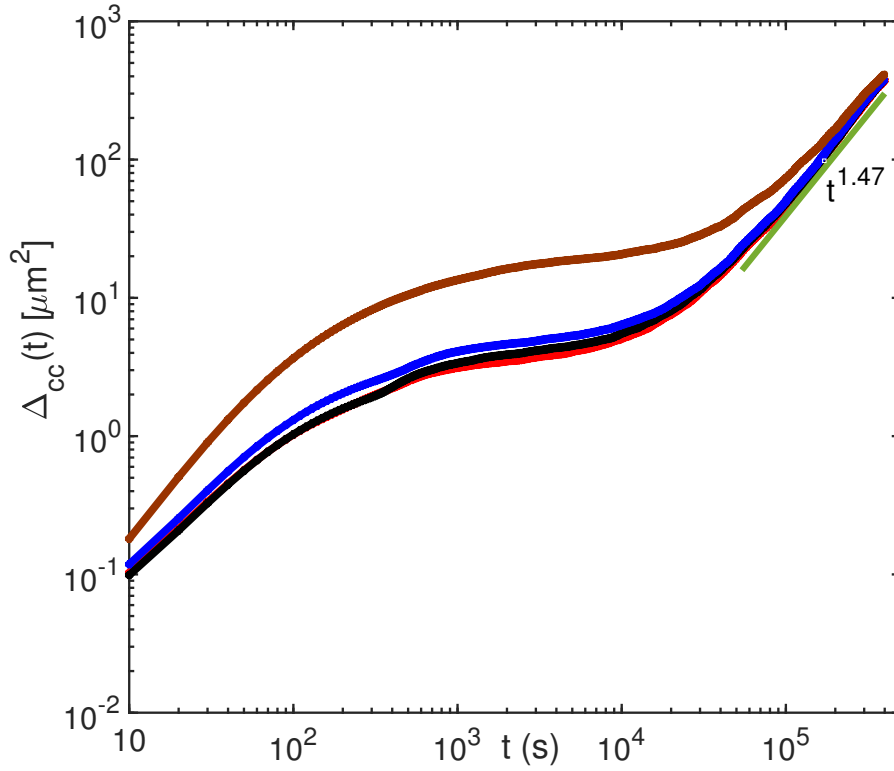


FIG. S5: CC dynamics under the influence of TPs. The mean-square displacement of the CCs (Δ_{CC}) using the Hertzian force (equation S13) as a function of time (t). From top to bottom, the curves correspond to different values of the radius of the TPs (brown $r_{TP} = 2r_c$, blue $r_{TP} = r_c$, black $r_{TP} = 0.75r_c$ (appears to be hidden) and red $r_{TP} = 0.5r_c$, where $r_c = 4.5 \mu m$ is the average cell radius). In the intermediate time limit, $\Delta_{CC}(t)$ is larger for TPs with larger radius. The green line is a guide to show the value of $\alpha_{CC}^S = 1.47$.

the CCs, the non-linearity arising from birth and apoptosis of the CCs determine super-diffusive behavior. In contrast, for the TPs, the TP-CC interaction term determines the hyper-diffusive behavior. This interaction coupled with the apoptosis-birth non-linear term in the cell density equation (Eq. (S5)), determines the dynamics of the TPs in the log-time limit.

Pressure profile: We calculated the radial pressure profile using simulations, which has been inferred [19] by compressing multicellular spheroids using the TPs as microsensors. As in the experiments the the pressure profile as the distance from the center of the tumor increases is monotonic, decreasing roughly by a factor of four. The pressure is almost constant in the core, and there is a gradual decrease (roughly by a factor of four) as the boundary of the tumor is reached (fig. (S6) in the pressure. The calculated pressure profile is in qualitative agreement with experiments [19]. The high pressure is due to small number cell division, which implies that the self-generated active (SGA) force is not large. As a consequence the CCs are jammed, leading to high internal pressure. As r increases CCs proliferate, resulting in an increase in the SGA, and consequently a decrease in the pressure (fig. (S6), and much higher mobility of the CCs near the periphery. Thus, there is an intimate relation between pressure profiles, and the tumor growth dynamics. It is remarkable that the simulated pressure profile is in qualitative but not quantitative agreement with experiments.

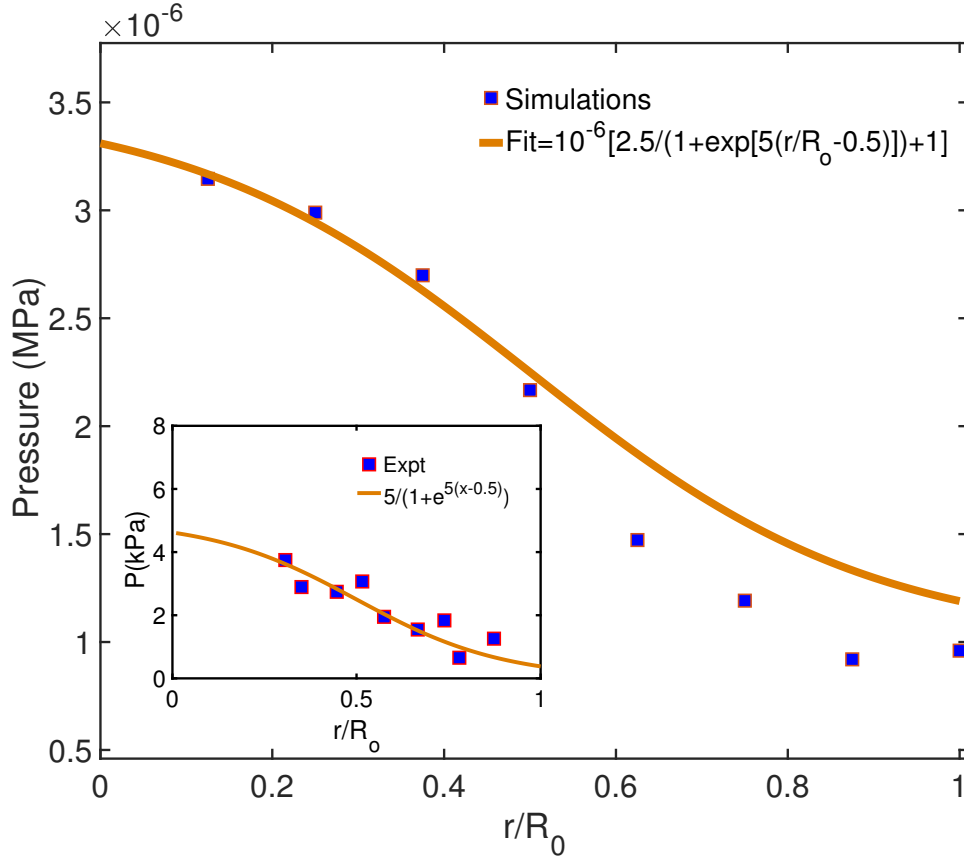


FIG. S6: Pressure as a function of radial distance within the simulated tumor. The pressure profile shows non-trivial dependence with the interior of the tumor being at high pressure with a gradual decay and can be approximated by a logistic function as shown by the fit. The pressure profile was calculated at the end of the simulation (400,000 s). The y-axis shows the value of pressure in MPa and the x-axis is the normalized radial distance. The inset shows the pressure profile as observed in experiments [19]. The fit to the experimental pressure profile has been approximated by a logistic function.

-
- [1] D. S. Dean, *J. Phys. A*, 1996, **29**, L613.
 - [2] M. Doi, *J. Phys. A: Math. Ge.*, 1976, **9**, 1465.
 - [3] L. Peliti, *J. Phys. (France)*, 1985, **46**, 1469.
 - [4] H. S. Samanta, M. Hinczewski and D. Thirumalai, *Phys. Rev. E*, 2017, **96**, 012406.
 - [5] H. S. Samanta and D. Thirumalai, *Phys. Rev. E*, 2019, **99**, 032401.
 - [6] C. Doering, C. Mueller and P. Smereka, *Physica A*, 2003, **325**, 243.
 - [7] A. Gelimson and R. Golestanian, *Phys. Rev. Lett.*, 2015, **114**, 028101.
 - [8] G. Parisi and Y. S. Wu, *Sci. Sin.*, 1981, **24**, 484.
 - [9] H. S. Samanta, J. K. Bhattacharjee and D. Gangopadhyay, *Phys. Letts. A*, 2006, **353**, 113.
 - [10] H. S. Samanta and J. K. Bhattacharjee, *Phys. Rev. E*, 2006, **73**, 046125.
 - [11] A. M. J. Valencia, P.-H. Wu, O. N. Yogurtcu, P. Rao, J. DiGiacomo, I. Godet, L. He, M.-H. Lee, D. Gilkes, S. X. Sun *et al.*, *Oncotarget*, 2015, **6**, 43438.
 - [12] A. N. Malmi-Kakkada, X. Li, H. S. Samanta, S. Sinha and D. Thirumalai, *Phys. Rev. X*, 2018, **8**, 021025.
 - [13] A. Malmi-Kakkada, X. Li, S. Sinha and D. Thirumalai, *arXiv preprint arXiv:1906.11292*, 2019.
 - [14] S. Sinha, A. Malmi-Kakkada, X. Li, H. Samanta and D. Thirumalai, *bioRxiv*, 2019, 842930.
 - [15] D. Drasdo and S. Höhme, *Phys. Biol.*, 2005, **2**, 133.
 - [16] G. Schaller and M. Meyer-Hermann, *Phys. Rev. E*, 2005, **71**, 051910.
 - [17] P. Pathmanathan, J. Cooper, A. Fletcher, G. Mirams, P. Murray, J. Osborne, J. Pitt-Francis, A. Walter and S. Chapman, *Phys. biol.*, 2009, **6**, 036001.

- [18] E. Palsson and H. G. Othmer, *Proc. Natl. Acad. Sci.*, 2000, **97**, 10448.
- [19] M. E. Dolega, M. Delarue, F. Ingremeau, J. Prost, A. Delon and G. Cappello, *Nat. Commun.*, 2017, **8**, 14056.
- [20] B. I. Shraiman, *roc. Natl. Acad. Sci.*, 2005, **102**, 3318–3323.
- [21] K. Alessandri, B. R. Sarangi, V. V. Gurchenkov, B. Sinha, T. R. Kießling, L. Fetler, F. Rico, S. Scheuring, C. Lamaze, A. Simon *et al.*, *roc. Natl. Acad. Sci.*, 2013, **110**, 14843–14848.
- [22] A. D. Conger and M. C. Ziskin, *Cancer Res.*, 1983, **43**, 556–560.
- [23] A. Puliafito, L. Hufnagel, P. Neveu, S. Streichan, A. Sigal, D. K. Fygenson and B. I. Shraiman, *roc. Natl. Acad. Sci.*, 2012, **109**, 739–744.
- [24] P. Gniewek, C. F. Schreck and O. Hallatschek, *Phys. Rev. Lett.*, 2019, **122**, 208102.